Pharm Res (2017) 34:1276–1295
DOI 10.1007/s11095-017-2144-0

RESEARCH PAPER

Impact of Micellar Surfactant on Supersaturation and Insight into Solubilization Mechanisms in Supersaturated Solutions of Atazanavir

Anura S. Indulkar[1] • Huaping Mo[2] • Yi Gao[3] • Shweta A. Raina[3] • Geoff G. Z. Zhang[4] • Lynne S. Taylor[1]

Received: 4 January 2017 / Accepted: 15 March 2017 / Published online: 28 March 2017

ABSTRACT

Purpose The goals of this study were to determine: 1) the impact of surfactants on the "amorphous solubility"; 2) the thermodynamic supersaturation in the presence of surfactant micelles; 3) the mechanism of solute solubilization by surfactant micelles in supersaturated solutions.

Methods The crystalline and amorphous solubility of atazanavir was determined in the presence of varying concentrations of micellar sodium dodecyl sulfate (SDS). Flux measurements, using a side-by-side diffusion cell, were employed to determine the free and micellar-bound drug concentrations. The solubilization mechanism as a function of atazanavir concentration was probed using fluorescence spectroscopy. Pulsed gradient spin-echo proton nuclear magnetic resonance (PGSE-NMR) spectroscopy was used to determine the change in micelle size with a change in drug concentration.

Results Changes in the micelle/water partition coefficient, $K_{m/w}$, as a function of atazanavir concentration led to erroneous estimates of the supersaturation when using concentration ratios. In contrast, determining the free drug concentration using flux measurements enabled improved determination of the thermodynamic supersaturation in the presence of micelles. Fluorescence spectroscopic studies suggested that $K_{m/w}$ changed based on the location of atazanavir solubilization which in turn changed with concentration. Thus, at a concentration equivalent to the crystalline solubility, atazanavir is solubilized by adsorption at the micelle corona, whereas in highly supersaturated solutions it is also solubilized in the micellar core. This difference in solubilization mechanism can lead to a breakdown in the prediction of amorphous solubility in the presence of SDS as well as challenges with determining supersaturation. PGSE-NMR suggested that the size of the SDS micelle is not impacted at the crystalline solubility of the drug but increases when the drug concentration reaches the amorphous solubility, in agreement with the proposed changes in solubilization mechanism.

Conclusions Micellar solubilization of atazanavir is complex, with the solubilization mechanism changing with differences in the degree of (super)saturation. This can result in erroneous predictions of the amorphous solubility and thermodynamic supersaturation in the presence of solubilizing additives. This in turn hinders understanding of the driving force for phase transformations and membrane transport, which is essential to better understand supersaturating dosage forms.

KEY WORDS amorphous solubility · crystalline solubility · micelles · solubilization mechanism · supersaturation · surfactants

ABBREVIATIONS

ASD	Amorphous solid dispersion
ATZ	Atazanavir
CMC	Critical micelle concentration
FRET	Förster resonance energy transfer
GLPS	Glass liquid phase separation
HPLC	High performance liquid chromatography
LLPS	Liquid liquid phase separation

✉ Geoff G. Z. Zhang
Geoff.GZ.Zhang@abbvie.com

✉ Lynne S. Taylor
lstaylor@purdue.edu

[1] Department of Industrial and Physical Pharmacy College of Pharmacy Purdue University 575 Stadium Mall Drive, West Lafayette Indiana 47907, USA

[2] Purdue Interdepartmental NMR Facility and Department of Medicinal Chemistry and Molecular Pharmacology Purdue University West Lafayette Indiana 47907, USA

[3] Manufacturing Science & Technology (MS&T), Operations AbbVie Inc. North Chicago, IL 60064, USA

[4] Drug Product Development, Research and Development AbbVie Inc. 1 N Waukegan Road North Chicago, IL 60064, USA

PGSE-NMR	Pulsed gradient spin-echo proton nuclear magnetic resonance
SDS	Sodium dodecyl sulfate

INTRODUCTION

The advent of computational chemistry and high throughput screening has resulted in major advances in the field of medicinal chemistry and drug discovery leading to a plethora of potential drug candidates (1–3). However, these advances have also led to challenges in the area of drug product development. New chemical entities advancing through discovery pipelines are trending towards higher molecular weights, melting points and/or lipophilicity, resulting in poor aqueous solubility (4,5). As solubility is an essential prerequisite for dissolution and oral bioavailability, formulation scientists are constantly searching for solubility enhancement strategies. Such strategies can be broadly classified into two categories. First, strategies that increase the drug concentration by enhancing crystalline solubility and second, strategies that generate supersaturated systems wherein the concentrations attained are higher than the crystalline solubility. Strategies such as solubilization by surfactant micelles (6) and complexation agents (cyclodextrins, albumin) (7,8) can be classified into the first category whereas, some lipid-based formulations (9–11), salts (12), cocrystals (13) and amorphous formulations (14) fall loosely under the second category. Supersaturated solutions can be generated if the formulation undergoes rapid dissolution generating concentrations higher than the crystalline solubility, or during gastrointestinal transit where weak bases can undergo a decrease in solubility on transit from the stomach to the small intestine. Further, conversion from a prodrug to the active drug has also been shown to result in supersaturation (15,16).

Supersaturated systems can offer certain advantages over the strategies that enhance the crystal solubility. Miller *et al.* and Dahan *et al.* determined the apparent permeability of progesterone at varying drug concentrations wherein higher apparent drug concentrations were achieved either by employing cyclodextrins, surfactants and cosolvents or by dissolution of an amorphous solid dispersion (ASD). It was observed that the techniques which increased the apparent crystalline solubility led to a decrease in membrane transport of the drug whereas, membrane transport was not sacrificed when an ASD was used to achieve high apparent concentrations (17–20). These observations can be readily explained by defining supersaturation in its true thermodynamic sense. It is well known that there is a quantitative relationship between the degree of supersaturation and the enhancement in penetration of the permeant across a membrane (21–24). Supersaturation, in rigorous thermodynamic terms, depends on the activity of the solute in the solution (25). In complex media, such as aqueous surfactant solutions, "free drug", as opposed to total drug, contributes to and dictates the drug activity. Thus, for the same total drug concentration, and at or below the LLPS concentration, the solute activity in the presence of solubilizing additives is lowered. As diffusion through a permeable membrane is driven by the solute activity gradient (26,27), solubilizing additives that reduce solute activity will negatively impact the transport of the drug across a membrane (28–30). This effect has to be balanced with the favorable effects of solubilizing additives in terms of promoting dissolution and enabling the drug to be present *in vivo* in a solubilized form.

It has been previously demonstrated that, in the absence of crystallization, highly supersaturated solutions of lipophilic drugs can undergo liquid-liquid phase separation (LLPS) or glass-liquid phase separation (GLPS) when the solution concentration exceeds the amorphous solubility, such that the concentration of the continuous phase corresponds to the amorphous solubility while the excess amorphous material (supercooled liquid or glass) precipitates as a dispersed phase. A metastable equilibrium exists between the two phases (31,32). The precipitated amorphous phase has been shown to exist in the form of drug-rich hydrophobic nanodroplets (31,33,34). The maximum flux is obtained at this concentration (35). At higher concentrations, the nanodroplets formed upon LLPS do not provide further enhancement in flux but have been demonstrated to sustain the maximum flux, acting as a reservoir to replenish molecularly dissolved drug removed by transport across the membrane, and maintaining the supersaturation at the amorphous solubility. Thus, LLPS, unlike crystallization which leads to desupersaturation and thus a decrease in the amount of drug available for absorption, can be potentially advantageous *in vivo* (36,37).

ASDs typically contain one or more drugs dispersed with a polymer and these formulations usually dissolve under non-sink conditions to produce a supersaturated solution. Additionally, surfactants may be added to improve the dissolution performance of the dispersion. For example, the commercially available ASDs, Kaletra® by AbbVie contains Span® 20, while Incivek® and Kalydeco®, both produced by Vertex Pharmaceuticals, contain sodium dodecyl sulfate (SDS). These surfactants are known to form micelles in aqueous media above the critical micelle concentration. Additionally, biorelevant media, popularly used as a surrogate for gastrointestinal (GI) fluids in *in vitro* studies contain mixed micelles formed by sodium taurocholate (STC) and lecithin (38,39). Human intestinal fluids have been shown to contain a multitude of bile salts as well as phospholipids (40). These bile salts, in combination with phospholipids, can form a variety of different structures such as micelles, mixed micelles and vesicles (41,42). Such structures can lead to solubilization of the drug and therefore, impact supersaturation (43,44). Raina *et al.*, observed that in supersaturated solutions containing

the same total drug concentration, at and below the LLPS concentration, solutions devoid of solubilizing agents exhibited higher drug flux than those containing solubilizing agents. While it was possible to increase the drug flux in the presence of solubilizing additives by increasing the total concentration of the drug, it was not straightforward to estimate the degree of supersaturation in these solutions. Additionally, while LLPS still occurred in the presence of solubilizing additives, this transition occurred at a higher total drug concentration as compared to in buffer, and the amorphous-to-crystalline solubility ratios were different in the presence and absence of solubilizing additives (45). These observations suggest that understanding the relationship between supersaturation and solubilization is not trivial. Due to the ubiquitous presence of surfactants, and the increasing utilization of supersaturating dosage forms, it is of great interest to gain a more fundamental understanding of amorphous solubility, supersaturation and solubilization mechanisms in the presence of surfactants.

It is commonly believed that a drug is solubilized in the hydrophobic micellar core, but reference to the literature shows that this view is an oversimplification. In his dissertation work, Feng showed that, for a group of chemically diverse molecules, the drug was solubilized at the micelle/water interface instead of micellar core at concentrations equivalent to the equilibrium solubility (46). In fact there are five sites on the micelle where the drug may be solubilized (47). Eriksson and Gillberg observed that for a given surfactant concentration, cetyltrimethylammonium bromide micelles solubilize benzene at different sites depending on the solute concentration suggestive of a change in solubilization mechanism (48). Thus, solubilization in the presence of surfactants may be a complex phenomenon with different modes of solubilization operating even for the same solute-surfactant system.

In this work atazanavir, a poorly water soluble compound, and sodium dodecyl sulfate (SDS), a widely used surfactant, (Fig. 1), are used to gain a fundamental understanding of supersaturation in the presence of surfactant micelles. We hypothesize that the micelle/water partitioning coefficient ($K_{m/w}$) changes as a function of drug concentration, leading to a complex relationship between supersaturation and concentration. Experimentally the hypothesis was tested by determining the $K_{m/w}$ as a function of solute concentration below (subsaturated) and above (supersaturated) the crystalline solubility. Additionally, fluorescence spectroscopy and nuclear magnetic resonance (NMR) studies were employed to gain insights into the solubilization mechanism(s).

MATERIALS

Atazanavir sulfate was purchased from Attix Corporation (Toronto, Canada). Methanol was obtained from Macron Fine Chemicals (Center Valley, PA). Curcumin was purchased from Spectrum Chemical Mfg. Corp. (Gardena, CA). Sodium dodecyl sulfate (SDS), pyrene carboxaldehyde, pyrene, dodecyl pyridinium chloride, deuterium oxide were obtained from Sigma-Aldrich (St. Louis, MO). Atazanavir free base (ATZ) was prepared following an established procedure (33). Briefly, a concentrated solution of ATZ sulfate prepared in methanol was added to a basic solution of NaOH to precipitate amorphous ATZ. This precipitate was then crystallized from a water:ethanol (1:1) mixture.

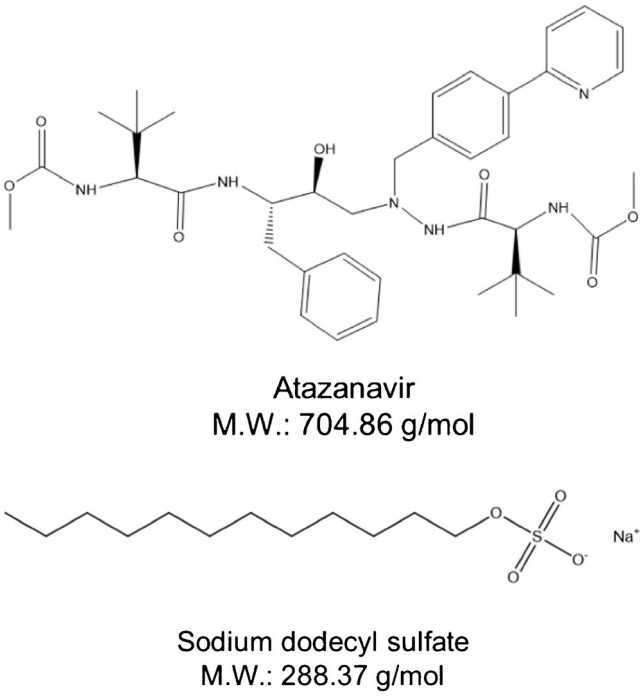

Fig. 1 Molecular structure and weight of atazanavir and sodium dodecyl sulfate.

METHODS

Determination of Micellar Properties of SDS

Critical Micelle Concentration (CMC)

The CMC of SDS was determined in 50 mM phosphate buffer pH 6.8 at 37°C by fluorescence spectroscopy using pyrene carboxyaldehyde as a fluorescent probe. Solutions of SDS in buffer ranging in concentrations between 0.05 and 2 mg/mL were prepared. Pyrene carboxyaldehyde was introduced by adding a methanolic solution (≤ 0.1 μg/mL) of the probe into the surfactant solution to achieve a final probe concentration of 0.5 μg/mL. The fluorescence spectrum was acquired for each surfactant solution using a Shimadzu RF-5301PC spectrofluorometer (Kyoto, Japan) at an excitation wavelength of 360 nm. The emission wavelength at the maximum intensity (λ_{max}) was recorded and the surfactant

concentration at which a change in λ_{max} was observed was taken as the CMC.

Micellar Aggregation Number (N_{agg})

N_{agg} for varying concentrations of SDS (1, 2 and 3.6 mg/mL) in pH 6.8 phosphate buffer at 37°C was determined by the static fluorescence quenching method. This method has been used extensively to determine N_{agg} (49–53). Here, pyrene was used as a fluorescent probe and dodecyl pyridinium chloride as the quencher. This probe-quencher combination has been previously reported for the SDS system (51). For a fixed surfactant concentration [C_{SDS}], pyrene was introduced into the aqueous medium by diluting the concentrated methanolic pyrene solution into the surfactant-containing buffer to yield a final pyrene concentration of 0.4 μg/mL (the added methanol concentration was ≤ 0.1 μg/mL). The intensity of the first emission peak of pyrene in the absence of the quencher was recorded (I_p) using a Shimadzu RF-5301PC spectrofluorometer (Kyoto, Japan) at an excitation wavelength of 332 nm. Next, varying concentrations of the quencher [Q], dodecyl pyridinium chloride were added to the SDS-pyrene solution and the emission intensity of the first peak was recorded at each quencher concentration (I_q). The N_{agg} was determined based on Eq. 1 (54).

$$ln\frac{I_p}{I_q} = \frac{[Q]N_{agg}}{[C_{SDS} - CMC]} \tag{1}$$

Plots of $ln\frac{I_p}{I_q}$ as a function of [Q] in molar units were made for each surfactant concentration and N_{agg} was determined from the slope.

Solubility Studies

Crystalline Solubility (S_{xtal})

The solubility of crystalline ATZ was determined in 50 mM phosphate buffer pH 6.8 both in the absence and presence of SDS. SDS solutions varying in concentrations between 0.05 to 3.6 mg/mL were prepared. To determine the crystalline solubility, an excess of crystalline solid was first equilibrated in the medium of interest for 48 h at 37°C followed by separation of solubilized drug by ultracentrifugation at 35000 rpm (209,490 g-force) using an Optima L-100 XP ultracentrifuge (Beckman Coulter, Inc., Brea, CA). The supernatant concentration was determined by high performance liquid chromatography (HPLC) with an Agilent 1260 Infinity system and an Agilent Eclipse Plus C18 5 μm, 2.1x150 mm column (Agilent Technologies, Santa Clara, CA). The mobile phase consisted of 60% pH 2.5 water acidified with o-phosphoric acid, and 40% acetonitrile. An injection volume of 15 μL was used and the flow rate was adjusted to 0.5 mL/min such that the retention time was less than 5 min. Detection was carried out at 210 nm using an ultraviolet (UV) detector. A calibration curve ($R^2 = 0.999$) constructed over the range 0.1 to 5 μg/mL was used for quantifying concentrations. Whenever necessary, dilution of the supernatant was carried out to obtain concentrations within the range of the calibration curve.

Predicted Amorphous Solubility (S_{pred})

The solubility advantage of the amorphous form over its crystalline counterpart is obtained because of the higher free energy of the amorphous form which in turn results from the lack of long range order in the solid. This difference in free energy (ΔG) can be estimated from the Hoffman equation in the dry state (Eq. 2) (55).

$$\Delta G = \frac{\Delta H_f (T_m - T)T}{T_m^2} \tag{2}$$

Here ΔH_f is the heat of fusion of the crystalline phase, T_m is the melting temperature of the crystal, and T is the temperature of interest (310 K).

Due to its disordered nature, the amorphous form of a compound has a tendency to absorb water which results in reduction in its thermodynamic activity. This leads to a decrease in the free energy difference and must be accounted for when estimating the solubility advantage. Thus, the predicted amorphous solubility (S_{pred}) can be estimated using Eq. 3 (56).

$$S_{\text{pred}} = exp\left[\frac{-\Delta G}{RT}\right]\exp[-I(a)]S_{\text{xtal}} \tag{3}$$

In this equation, the term, $exp\left[\frac{-\Delta G}{RT}\right]$ takes into account the solubility advantage due to the lack of crystalline structure; whereas the term $\exp[-I(a)]$ is a correction factor that considers the decrease in thermodynamic activity due to water. The amount of water can be obtained from the moisture sorption isotherms of the amorphous form. This approach of predicting amorphous solubility has been applied to numerous pharmaceutical compounds, and generally provides good estimates (31,57).

A TA Q2000 differential scanning calorimeter (DSC) with a refrigerated cooling accessory (TA Instruments, New Castle, DE) was used to determine the T_m and ΔH_f of crystalline ATZ. The drug was heated in the DSC from 10°C to 250°C at a heating rate of 5°C/min and a nitrogen flow of 50 mL/min was maintained to create a dry environment. Amorphous ATZ was prepared by melting crystalline ATZ and quench cooling the melt with liquid nitrogen. A symmetric vapor sorption analyzer SGA-100 (VTI Instruments, Irvine, CA) was used to obtain moisture sorption profiles of amorphous ATZ by placing approximately 15 mg of the drug in sample pan followed by drying at 37°C. The relative humidity was

increased from 5 to 95% with a 5% interval and the corresponding weight gain by the sample due to moisture sorption at 37°C was recorded. A weight equilibration criterion of less than 0.01% weight change over a 10 min period was used to determine the equilibration time at a particular RH. The term $\exp[-I(a)]$ was determined from the percentage weight gain with increases in relative humidity data using the method described by Murdande *et al.* (56). S_{pred} in absence or presence of SDS was determined using Eq. 3 and employing S_{xtal}.

Experimental Amorphous Solubility/ LLPS Concentration (S_{LLPS})

The experimental amorphous solubility or the onset of LLPS was determined using the solvent shift method (31). Although GLPS is an appropriate terminology for atazanavir since the glass transition temperature of the amorphous precipitate equilibrated with water is higher than the experimental temperature (33), the term LLPS is employed in this work as it is more commonly used to describe amorphous phase separation in aqueous media. Aqueous solutions of SDS in pH 6.8 buffer were prepared over the concentration range of 0.05 to 3.6 mg/mL and equilibrated at 37°C. A concentrated solution of the drug prepared in methanol (30 mg/mL) was then diluted into the aqueous surfactant solutions at a particular rate using a syringe pump to generate supersaturated solutions. The rate of addition of this solution into aqueous medium was varied such that the duration of experiment was less than 10 min. Supersaturated solutions of varying concentrations thus generated were constantly stirred at 300 rpm and monitored for changes in scattering by measuring extinction at a non-absorbing wavelength of 350 nm using a UV/vis spectrophotometer (SI Photonics, Tuscon, Arizona), coupled with a fiber optic dip probe. The concentration at which a sharp change in the slope of a plot of scattering as a function of concentration was observed was taken as the LLPS concentration or experimental amorphous solubility.

Determination of Diffusive Flux

Diffusive flux was determined both in pH 6.8 phosphate buffer and buffer containing predissolved SDS using a side-by-side diffusion cell (PermeGear Inc., Hellertown, PA). To study the impact of the surfactant, varying concentrations of SDS, 1, 2 and 3.6 mg/mL were employed. The diffusion cell consisted of a donor compartment separated from the receiver compartment by a Spectra/Por® 1 regenerated cellulose membrane (Spectrum Laboratories Inc., Rancho Dominguez, CA) with molecular weight cut off value of 6–8 kD. 34 mL of the aqueous medium was added to both the donor and the receiver compartments and equilibrated at 37°C. The surface area of the membrane available for mass transport was 7.07cm^2. A concentrated stock solution of the drug (30 mg/mL) prepared in methanol was then diluted into the donor side to achieve the desired total drug concentration. The concentration of the drug permeated to the receiver side was monitored by withdrawing 200 μL of aliquots every 10 min over the 60 min duration of the experiment and determining the concentration using HPLC.

Diffusive flux (J), which by definition is the rate of mass transfer per unit surface area, is given by the Eq. 4.

$$J = \frac{dm}{Adt} \tag{4}$$

Here, $\frac{dm}{dt}$ is the rate of mass transfer and A is the cross sectional area of the membrane. Hence, the concentration achieved on the receiver side was plotted as a function of time for each initial donor concentration. The slope of each plot was then converted to flux (J) by factoring in the total volume of the medium and the cross sectional area of the membrane.

Fluorescence Spectroscopy

As ATZ is an autofluorescent molecule, fluorescence spectroscopy was carried out on ATZ solutions prepared in pH 6.8 phosphate buffer as well as in the presence of 1, 2 and 3.6 mg/mL SDS solutions using a Shimadzu RF-5301PC spectrofluorometer (Kyoto, Japan). The final drug concentration in the medium ranged from less than the crystalline solubility (subsaturated systems) up to the LLPS concentration (highly supersaturated systems). Desired concentrations of the drug were achieved by diluting a concentrated methanolic solution of the drug into the medium. An excitation wavelength of 250 nm was used and changes in emission spectra were recorded. A solid state emission spectrum of a thin amorphous film ATZ was also obtained to observe the major emission peaks when the interactions exist solely between the drug molecules. Solid-state fluorescence has been previously used to study the environment around the drug using fluorescent probes (58). Briefly, 100 μL of a 30 mg/mL of drug solution prepared in methanol was placed on quartz cover glass and a thin film was obtained by spin coating using a KW-4A spin coater (Chemat Technology Inc., Northridge, CA) and rotating at 3000 rpm for 30s.

To elucidate the location of solubilization of the drug in SDS micelles, Förster resonance energy transfer (FRET) experiments were carried. Curcumin was used as a FRET partner for ATZ as curcumin shows fluorescence emission only when excited at 369 nm and does not emit when excited at 250 or 328 nm. Here, curcumin was dissolved in 3.6 mg/mL SDS solution to give final curcumin concentration of 0.5 μg/mL. Emission spectra of curcumin alone in a 3.6 mg/mL SDS solution were recorded at excitation wavelengths of 250, 328 and 369 nm. Three different wavelengths were used here to ensure that curcumin does not exhibit fluorescence when excited at 250 and 328 nm but fluoresces when excited at

369 nm. ATZ was added to the curcumin-containing SDS solution in the concentration range between 45 to 1200 μg/mL by pipetting an aliquot of concentrated methanolic drug solution sufficient to attain the desired concentration. Fluorescence measurements of these solutions were carried out using an excitation wavelength of 250 nm and emission spectra were collected with the aim of detecting the emergence of a curcumin emission peak indicating a FRET effect.

Size Determination of SDS Micelles

The self-diffusion co-efficient (D_{NMR}) of the micelles was determined using pulsed gradient spin-echo proton NMR (PGSE-NMR). Measurements were performed at 25°C on a Bruker 500 MHz (^{1}H) spectrometer equipped with a triple resonance inverse z-gradient cryogeneic probe. A lower temperature was used here to avoid crystallization of the drug, as crystallization kinetics are slower at reduced temperatures. A stimulated spin-echo with longitudinal eddy decay was employed for the measurement. Gradient strength was 6 G/mm with a D_2O sample as the standard. For each D_{NMR} measurement, gradient strength was linearly increased from 2% to 95% of the full strength in 16 steps; a relaxation delay of 10 s was used and 8 scans were accumulated for each gradient strength. 40 mg/mL of SDS solution was prepared in D_2O containing phosphate salts at a concentration of 50 mM. Higher SDS concentration was employed to minimize the contribution of the monomers towards D_{NMR}. At this concentration, only 1.25% of SDS molecules are present in the monomeric form. 600 μL of the sample was placed in a NMR tube and measurements for micellar D_{NMR} were carried out both in absence and presence of two different ATZ concentrations viz. 0.4 mg/mL and 7 mg/mL. The size of the micelles was then calculated from D_{NMR} by employing the Stokes-Einstein equation (Eq. 5).

$$D_{NMR} = \frac{k_B T}{6\pi\eta r} \tag{5}$$

Here, T is the experimental temperature (25°C), k_B is the Boltzmann constant, η is the viscosity of the medium which was taken as the viscosity of water at 25°C assuming the surfactant and the drug do not change the viscosity of the medium, and r is the hydrodynamic radius of the micelle.

RESULTS

Determination of Micellar Properties of SDS

Critical Micelle Concentration (CMC)

It is well known that the CMC of an ionic surfactant is impacted by the presence of salts and the ionic strength of the solution (59,60). Hence, the CMC of SDS was determined in the medium of interest for this study, 50 mM pH 6.8 phosphate buffer at 37°C using an environment sensitive fluorescent probe, pyrene carboxyaldehyde. In principle, at concentrations where the surfactant exists as monomers, the probe is distributed uniformly in the aqueous medium and hence senses a polar environment, whereas when the surfactant exists as aggregates/micelles, the hydrophobic probe partitions into the hydrophobic core of the micelle and now senses a relatively less polar environment (61). This change in polarity leads to a change in the probe emission characteristics such as the intensity at λ_{max} or the λ_{max}. Generally, a hypsochromic (blue) shift in λ_{max} is observed when the environment changes from polar to non-polar. Figure 2a shows the λ_{max} of pyrene carboxyaldehyde plotted as a function of varying SDS concentrations. It is evident that the λ_{max} changes at an SDS concentration of 0.5 mg/mL, and this concentration was taken as the CMC of SDS for the above mentioned experimental conditions. The CMC of SDS in water is known to be 2.4 mg/mL (62). The lower value obtained in this work is attributed to the increase in ionic strength due to presence of buffer ions. This CMC value is very similar to that reported by Fuguet *et al.* in medium containing a 50 mM concentration of electrolytes (59).

Micellar Aggregation Number (N_{agg})

N_{agg} was determined using the static fluorescence quenching method (51–54). Figure 2b shows a plot of $ln\left(\frac{I_p}{I_f}\right)$ as a function of quencher concentration [Q] for 3.6 mg/mL of SDS. The method is based on the principle that both the quencher and the fluorescent probe can partition into the micelles and that the distribution follows Poisson statistics (54). Further, if the probe and quencher coexist in the same micelle, the probe will not contribute to the total emission intensity i.e. emission intensity will be recorded only from the micelles that contain the probe but not the quencher. Using Fig. 2b and Eq. 1, N_{agg} was determined to be 65. The same method was used to determine the N_{agg} values at 1 and 2 mg/mL SDS concentrations which were found to be 60 and 58 respectively. These results are consistent with previously reported values (51,63). Further, it can be noted that the N_{agg} values do not drastically change with increasing SDS concentration. This result is also in line with earlier reports that SDS micelles are slow growing and that there is an increase in the number of micelles with concentration while the N_{agg} remains fairly constant (63).

Solubility Studies

The crystalline solubility of atazanavir at 37°C in pH 6.8 phosphate buffer was found to be 1.1 μg/mL. The thermodynamic parameters employed to determine the predicted amorphous solubility are presented in Table I. Based on these parameters, the ratio of the predicted amorphous solubility to

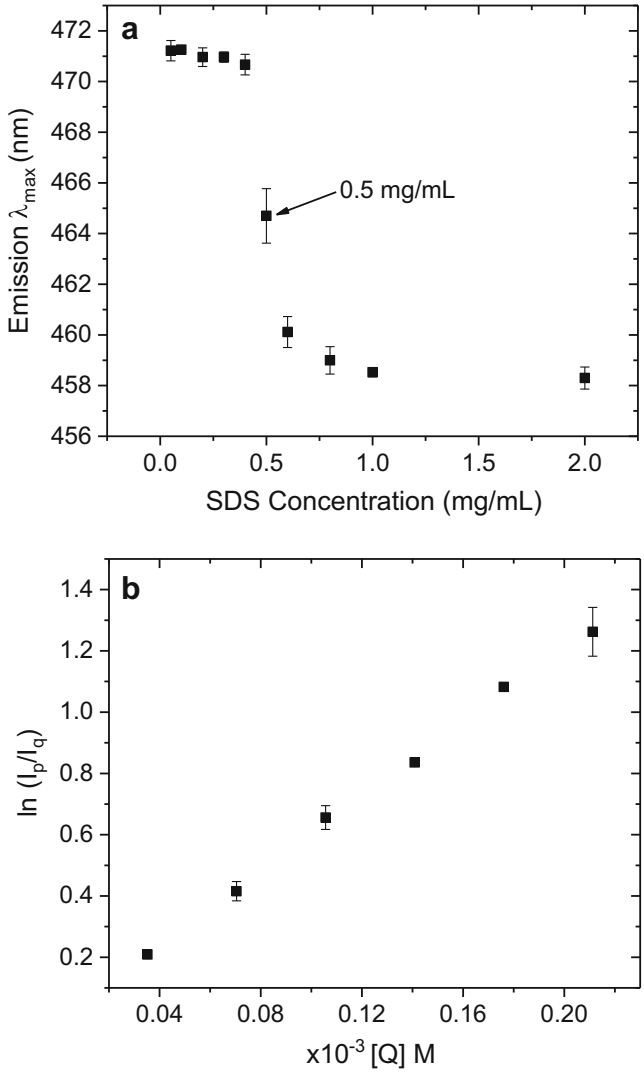

Fig. 2 Determination of micellar properties of SDS. (**a**) Critical micelle concentration (CMC) of SDS at 37°C in 50 mM pH 6.8 buffer using pyrene carboxyaldehyde as a fluorescent probe. Decrease in emission λ_{max} is observed at 0.5 mg/mL suggestive of micelle formation. (**b**) aggregation number (N_{agg}) of SDS by static fluorescence quenching using pyrene as a fluorescent probe and dodecyl pyridinium chloride as a quencher. N_{agg} can be estimated from the slope of the plot and concentration of micellized surfactant.

the crystalline solubility was found to be 62 and the predicted amorphous solubility or the maximum solubility that ATZ can attain prior to liquid-liquid phase separation was estimated to be 68 μg/mL. The experimental amorphous solubility or the LLPS concentration determined by the solvent shift method was found to be 70 μg/mL in surfactant-free buffer which is in excellent agreement with the predicted amorphous solubility. Thus, for ATZ it is apparent that the maximum solubility advantage can be achieved experimentally. This theoretical or maximum solubility advantage may not be achieved by all compounds due to crystallization.

Table I Thermodynamic Parameters of ATZ Employed in the Determination of Predicted Amorphous Solubility

T_m (°C)	ΔH_f (J/g)	Moisture absorbed (%)	I (a)
208	90.1	5.2	0.22

The crystalline solubility as a function of SDS concentration is presented in Fig. 3. It can be seen that the solubility remains approximately constant at around 1 μg/mL up to an SDS concentration of 0.5 mg/mL. Above this, a linear increase in solubility is observed. This result is in excellent agreement with the CMC determined in this work. At the CMC, micelles begin to form, and as a result, solubility enhancement is observed when this concentration is exceeded as the micelles can solubilize the drug. A similar trend was observed for the LLPS concentration determined at varying surfactant concentrations (Fig. 4). From the increase in the solubility of crystalline ATZ, the predicted amorphous solubility also can be estimated and compared to the experimentally determined amorphous solubility (Fig. 4). The total solubility (S) observed in presence of a surfactant is given by Eq. 6 (64).

$$S = S_0 + \kappa(C_{SDS} - CMC) \tag{6}$$

Here, S_0 is the solubility of the drug in the absence of surfactant (either crystalline or amorphous solubility as appropriate), κ is the molar solubilization ratio or the solubilizing power of the surfactant and C_{SDS} is the total SDS concentration. Thus, the term C_{SDS}-CMC represents the concentration of surfactant molecules in the micellar state. Figure 4 presents three solubility profiles plotted as a function of micellized SDS concentration. It is evident that the experimental amorphous solubility is higher than the crystalline solubility but does not reach the predicted amorphous solubility limit (calculated from the crystalline

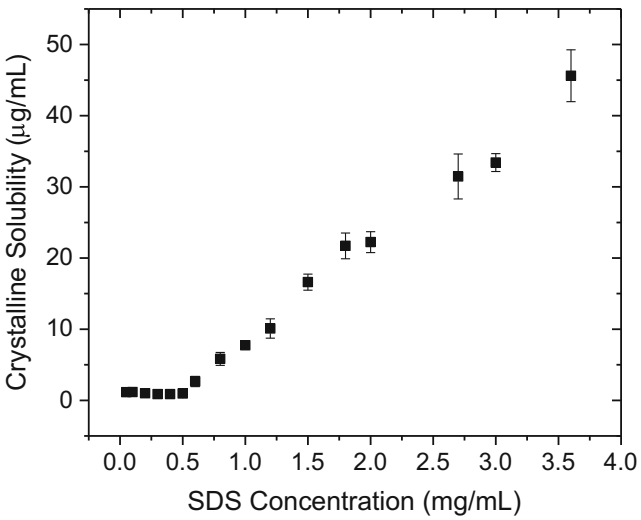

Fig. 3 Crystalline solubility of ATZ in the presence of varying SDS concentrations at 37°C in 50 mM pH 6.8 buffer. Increase in crystalline solubility is observed above the CMC of SDS.

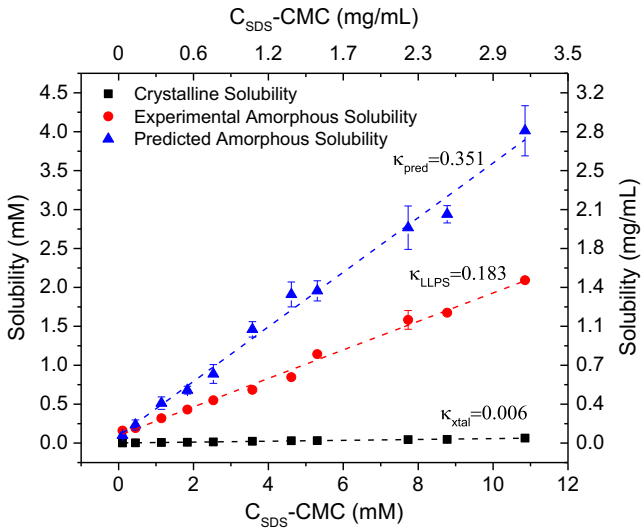

Fig. 4 Comparison of crystalline, predicted amorphous and experimental amorphous solubility values of ATZ in presence of SDS. The slope gives the molar solubilization ratio (κ) for different solubility profiles. Secondary axes shows the concentrations in *w/v* units.

solubility at the SDS concentration of interest and Eq. 3). Based on fitting the data in Fig. 4 to Eq. 6, κ and S_0 values were determined from the slope and intercept respectively, and are presented in Table II. S_0 values from the plot were also compared to the experimentally determined solubility values in the absence of SDS (Table II). Two observations can be made: 1) based on a comparison of S_0 values, it is apparent that the Eq. 6 can be satisfactorily applied to model the solubilization of both the crystalline and amorphous forms; 2) the solubilizing power of the surfactant for the amorphous form is different from that for the crystalline form. Hence, Eq. 3 which gives excellent correlation between solubility values for predicted and experimental amorphous solubility in pure aqueous buffer, fails to predict the total solubility enhancement of the amorphous form in presence of SDS.

Determination of Solute Activity and Supersaturation Ratio in Presence of SDS

Diffusive flux experiments carried out using side-by-side diffusion cell were used to determine the activity of the drug in the solution. Figure 5 shows a plot of flux as a function of varying total ATZ concentrations added to the donor compartment in absence of surfactants. It can be seen that the flux increases linearly with an increase in ATZ donor concentration from the crystal solubility to the amorphous solubility. For donor concentrations added in excess of the amorphous solubility, the flux reaches a plateau. This occurs because, in rigorous thermodynamic terms, the flux, J, is directly proportional to the activity (a) of the solute in the solution (Eq. 7) (26). Here D is the diffusion coefficient of the solute, h is the membrane thickness and γ_m is the activity coefficient of the solute in the membrane.

$$J = \frac{Da}{h\gamma_m} \tag{7}$$

Activity is directly related to concentration, c, by Eq. 8

$$a = \gamma c \tag{8}$$

Where γ is the activity coefficient of the solute in the aqueous phase. In dilute concentration regime (concentrations up to the amorphous solubility where the solution is expected to behave as an ideal dilute solution), $\gamma = 1$, and activity can be substituted by concentration. However, at concentrations exceeding the amorphous solubility, the excess drug separates into a second amorphous phase. In this case, the solute activity is equal to the activity of a solute in a solution with a concentration corresponding to the amorphous solubility. Similar trends in flux versus concentration plots have been previously observed with supersaturated felodipine and nifedipine systems (35). The plot of flux as a function of concentration in the region up to the amorphous solubility in surfactant-free buffer, where $\gamma = 1$ (a linear fit to the data in Fig. 5 gave an R^2 value of 0.998 and a slope of 0.0017 mL/min.cm^2) was then used as a calibration curve to determine the activity of the drug in the presence of varying SDS concentrations between the limits of the crystal and amorphous solubility. This approach of estimating the free solute concentration (i.e. the solute activity) in the presence of surfactant micelles is similar to the dialysis approach employed for the same purpose (65,66). Fig. 6 shows ATZ free drug concentration as a function of total ATZ concentration in the absence of SDS, and in the presence of 1, 2, and 3.6 mg/mL SDS. It is apparent that the free drug concentration ranges between ~1 μg/mL at the

Table II Summary of Solubilizing Capacity (κ) of SDS and Solubility Values in Pure Buffer (S_0) for Different Solubility Profiles

	Crystalline	Experimental amorphous	Predicted amorphous
κ	0.006	0.183	0.351
*S_0 from plot (μg/mL)	1.04	64.6	69.2
S_0 experimental (μg/mL)	1.08	67.5	70

*values obtained from Figure 4

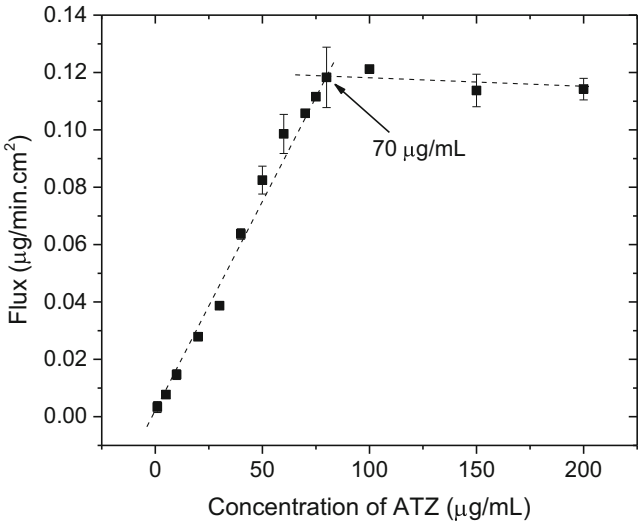

Fig. 5 Flux of ATZ in 50 mM pH 6.8 buffer at 37°C for varying ATZ concentrations. The flux reaches a maximum at the amorphous solubility.

crystalline solubility and ~65 μg/mL at the amorphous solubility both in absence and presence of SDS, even though the total solution concentrations are drastically different.

Next, the supersaturation ratio (*SR*) was determined for all the above mentioned systems. By definition, *SR* is the ratio of activity of the solute (*a*) in a solution to the activity of the solute at saturation (crystal solubility) (a^*) (25). From this definition and from Eq. 8, *SR* is given by:

$$SR = \frac{a}{a^*} = \frac{\gamma c}{\gamma^* c^*} \tag{9}$$

The superscript "*" represents the properties of the system at saturation. Typically within pharmaceutical sciences, when

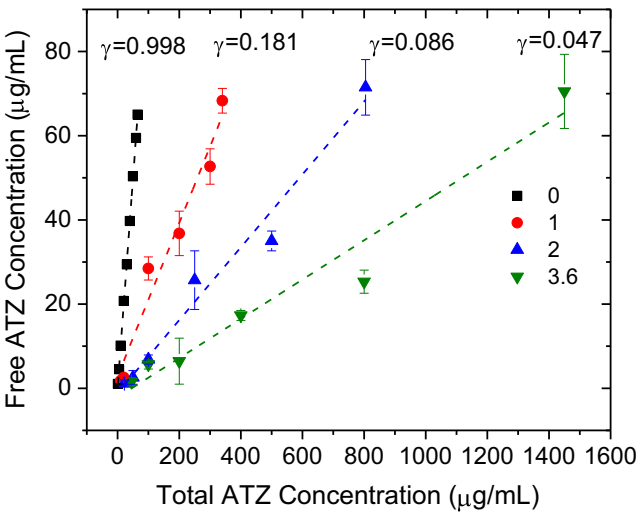

Fig. 6 ATZ free drug concentration as a function of total ATZ concentration for varying SDS concentrations. Free drug concentration varies between 1 μg/mL at the crystalline solubility and 65 μg/mL at the amorphous solubility. γ = 1 in absence of SDS and decreases with increasing SDS concentrations. γ is estimated assuming ideal dilute solution as standard state.

studies of supersaturation are conducted in both simple and complex media, γ / γ^* is assumed to be 1, and activity is substituted by concentration terms to determine *SR*. Thus the solubility of the crystalline form is determined in the medium of interest (simple buffer, or complex medium containing surfactants), and the *SR* is determined using this value. To demonstrate that this oversimplification may not always be accurate in terms of describing the fundamental supersaturation, *SR* based on the ratio of activities ($SR_{activity}$) was compared to the *SR* derived from the ratio of concentrations (SR_{conc}). For the concentration-based *SR* values, the total ATZ concentration and the crystalline solubility in the medium of interest was used. For the activity-based *SR* values, the flux data was used to estimate the drug activity in the medium of interest. Figure 7a shows the *SR* determined by the two methods for 3.6 mg/mL SDS solutions containing varying ATZ concentrations between the crystalline and amorphous solubility values. Figure 7b shows the *SR* determined at the amorphous solubility for varying SDS concentrations and a comparison of the *SR* determined in the absence of SDS. As expected, in the absence of SDS, the SR_{conc} and $SR_{activity}$ are equal. However, when solubilizing additives are present and $\gamma / \gamma^* \neq 1$, these two ratios are not equal. SR_{conc} clearly underpredicts the fundamental supersaturation. In contrast, $SR_{activity}$ varies between 1 at the crystalline solubility and 65 at the amorphous solubility (within experimental error) regardless of SDS presence. These results provide confirmation that the flux method provides a good estimation of the fundamental supersaturation since the predicted activity ratio between the crystalline and amorphous forms of ATZ is 62, in excellent agreement with the experimentally determined $SR_{activity}$ value of 65.

Mechanism of Solubilization: Determination of $K_{m/w}$

The micelle to water partition coefficient ($K_{m/w}$) of the drug was determined at different ATZ concentrations using Eq. 10:

$$K_{m/w} = \frac{[drug\ in\ the\ micelle]}{[free\ drug\ in\ aqueous\ compartment]} \tag{10}$$

The concentration of the free drug (drug in aqueous compartment) was obtained from the diffusive flux experiments as described above. The concentration of the drug in the micelle was then obtained by mass balance since the total drug concentration was known. Figure 8 shows a plot of $K_{m/w}$ as a function of ATZ concentrations added to a 3.6 mg/mL SDS solution and it is readily apparent that $K_{m/w}$ is not a constant. This plot can be divided in to two regions. Region I, in which $K_{m/w}$ decreases linearly with an increase in total drug concentration up to a concentration slightly above the crystal solubility, and Region II where the $K_{m/w}$ is observed to reach a relatively constant value. Similar graphs were plotted for other SDS concentrations and it was observed that the change in

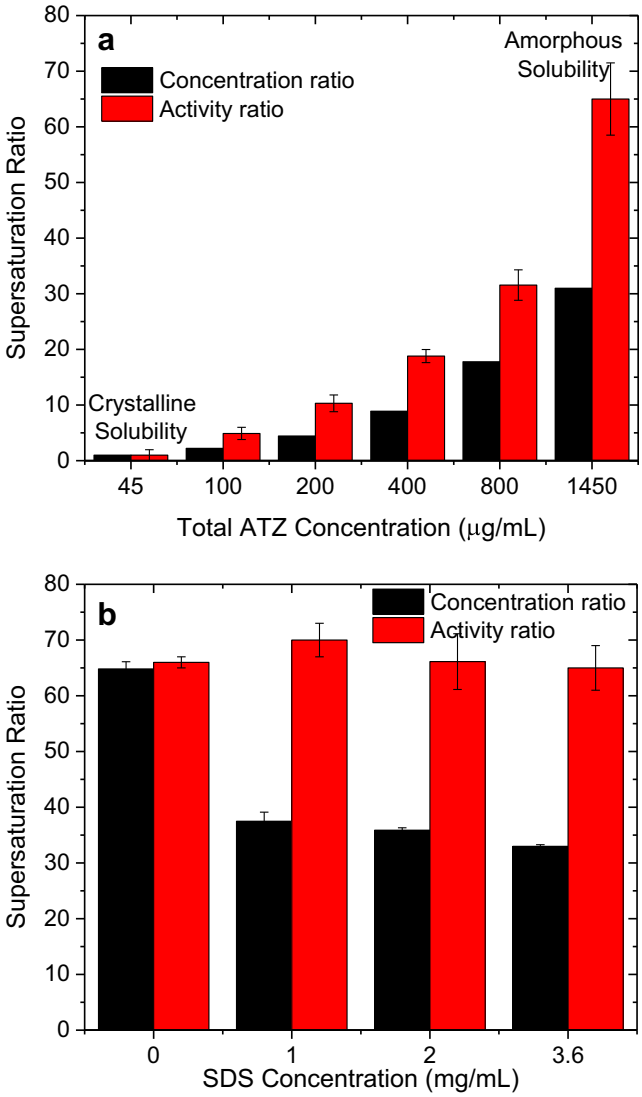

Fig. 7 Comparison of concentration and activity based supersaturation ratio (SR). (**a**) SR as a function of total ATZ concentration in presence of 3.6 mg/mL SDS. The activity-based SR varies between 1 at the crystalline solubility and 65 at amorphous solubility whereas the concentration-based SR varies between 1 and 30. (**b**) SR at the amorphous solubility at various SDS concentrations, Activity-based SR is ~65 whereas concentration based SR is ~30.

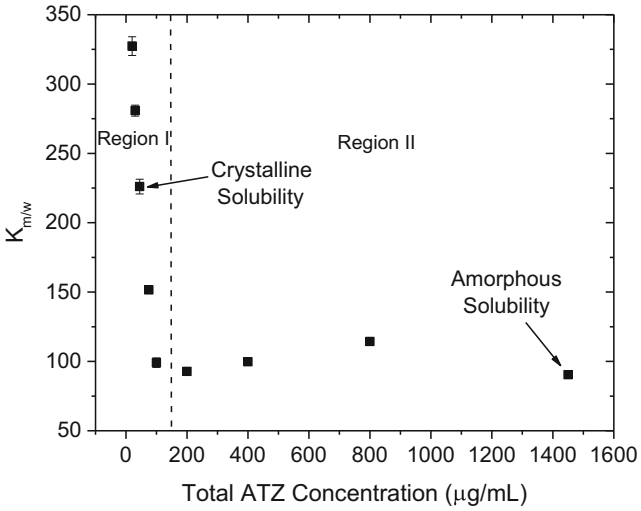

Fig. 8 Plot of micelle/water coefficient ($K_{m/w}$) as a function of varying ATZ concentrations in presence of 3.6 mg/mL SDS. $K_{m/w}$ decreases with ATZ concentration in region I where the drug is solubilized by adsorption at the micelle interface whereas, it reaches a plateau in region II where the drug is solubilized by dissolution in the core.

slope of $K_{m/w}$ occurs at the same activity regardless of the surfactant concentration (data not shown). A trend similar to that observed in Region I was reported for nystatin in presence of Cremophor EL and Nofable ESO-9920, whereas a trend similar to Region II was observed for pyrene in the same surfactant systems (67). The authors concluded that these differences result because of different solubilization mechanisms at play for the two solutes wherein, nystatin is solubilized by adsorbing at the interface of the hydrophilic corona and hydrophobic core, whereas pyrene is solubilized by partitioning into the hydrophobic core. In this study, these two trends were observed for the same solute but at different levels of sub/supersaturation. Hence, we can speculate that the ATZ molecule is solubilized by adsorption at the interface when the total solution concentration is near the saturation solubility, while above this concentration, when the adsorption sites are saturated, the drug is solubilized by association with the hydrophobic core. This speculation is supported by the observation that Region I could be fit to the Langmuir adsorption isotherm (Eq. 11) (64):

$$\frac{C}{x} = \frac{1}{K_{ad} x_m} + \frac{C}{x_m} \tag{11}$$

Here, C is the molar concentration of free solute molecules, x is the solute mole fraction in the micellar phase, x_m is the maximum solute mole fraction adsorbed and K_{ad} is the Langmuir adsorption constant. Figure 9 shows a plot of $\frac{C}{x}$ as a function of C for the Region I. The plot follows a linear trend with an R^2 value of 0.998 and K_{ad} value of 3.86 x 10^5 L/mol. x_m determined from the slope of the plot was found to be 0.017 and corresponds to a total ATZ concentration of 130 μg/mL which is very close to the concentration at which the solubilization mechanism changes from adsorption to dissolution based on Fig. 8. Further evidence for a change in solubilization mechanism in supersaturated ATZ solutions is provided below.

Mechanism of Solubilization: Fluorescence Spectroscopy

Fluorescence studies were conducted to further investigate the ATZ environment in the surfactant micelles. ATZ is autofluorescent, and like many fluorescent molecules, the

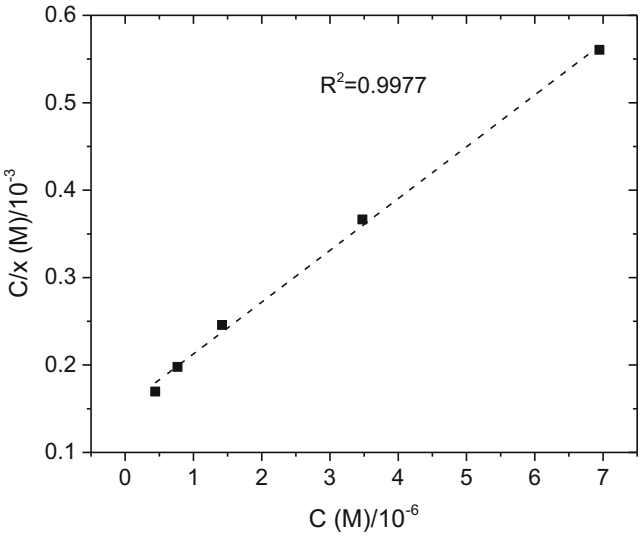

Fig. 9 Langmuir adsorption isotherm for ATZ in 3.6 mg/mL SDS corresponding to Region I in Figure 8.

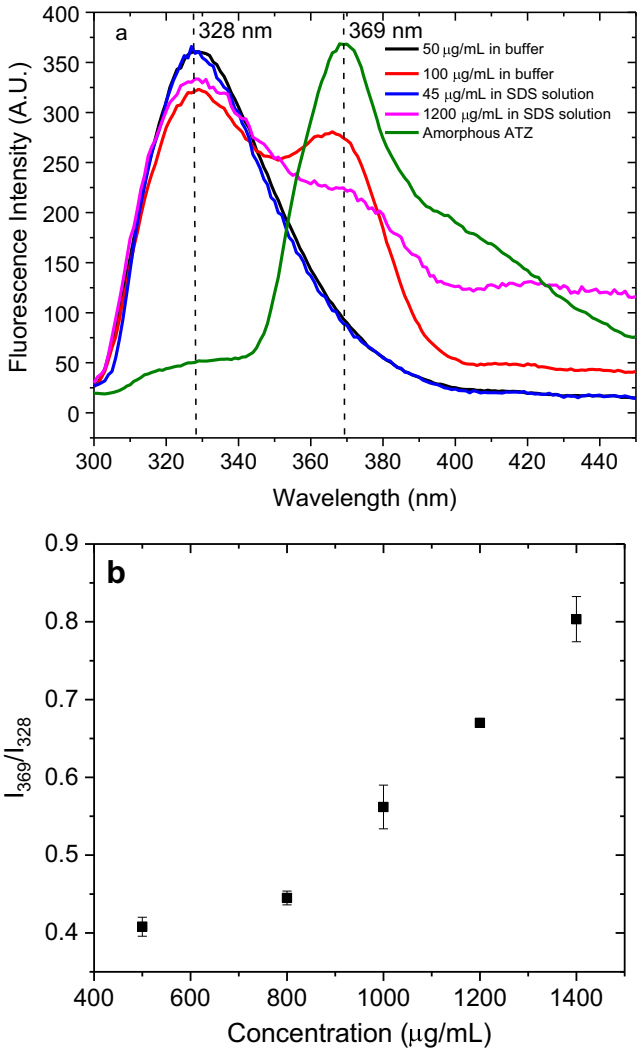

Fig. 10 (**a**) Fluorescence emission spectra of ATZ in different environments using an excitation wavelength of 250 nm. Numbers show the two λ_{max} obtained for different systems. (**b**) Relative fluorescence intensity of the two peaks at 328 and 369 nm for varying ATZ concentrations in Region II in the presence of 3.6 mg/mL SDS. Increase in I_{369}/I_{328} suggests an increase in self-interaction of drug molecules due to localization.

emission spectrum is expected to vary depending on the environment. Figure 10a shows the emission spectra of ATZ in different environments. At a concentration of 50 μg/mL which is lower than the amorphous solubility of the drug in pH 6.8 buffer, the drug exhibits a single emission peak at 328 nm (black curve in Fig. 10a). This is representative of an emission spectrum in a dilute polar aqueous environment. In a less polar concentrated environment where the ATZ molecules are highly aggregated as in an amorphous film of the drug, the drug exhibits an emission peak at 369 nm (green curve in Fig. 10a). When the amorphous solubility of the drug in buffer is exceeded (corresponding to red curve in Fig. 10a), the emission spectrum shows peaks at both 328 and 369 nm. In this case, the drug molecules dissolved in the buffer sense a polar environment and contribute to the peak at 328 nm whereas, the drug molecules in the disordered ATZ-rich phase which sense a less polar environment emit at 369 nm. In a 3.6 mg/mL SDS solution, when the drug concentration is equal to 45 μg/mL corresponding to Region I of solubilization, the drug emits a single peak at 328 nm (blue curve in Fig. 10a) whereas, when the drug concentration is increased to 1200 μg/mL which is still lower than the amorphous solubility of the drug but corresponds to Region II of solubilization, the drug exhibits two emission peaks at 328 and 369 nm (magenta curve in Fig. 10a). For a range of ATZ concentrations studied in presence of SDS, the second emission peak was evident only when the drug concentration exceeded 200 μg/mL. Figure 10b shows the relative emission intensities at the two wavelengths for varying ATZ concentrations in Region II in the presence of 3.6 mg/mL SDS plotted as the emission intensity ratio of the peak at 369 nm to that of the peak at 328 nm (I_{369}/I_{328}). I_{369}/I_{328} increases with increasing ATZ concentration. The emergence of the peak at 369 nm and the subsequent increase in intensity with increasing ATZ concentration, suggests that ATZ molecules are undergoing self-interactions. As this peak becomes evident at concentrations well below the experimentally determined amorphous solubility, this peak is not due to phase separation to a drug-rich phase. The observed trends support the proposed change in solubilization mechanism of ATZ by SDS. In Region I, when the drug is solubilized by adsorption at interface, it can still sense the aqueous environment resulting in a single emission peak occurring at 328 nm – this peak has contributions from ATZ molecules dissolved in solution, as well as those adsorbed at the micelle-water interface. However, when the concentration of the drug in the micellar core increases (Region II), drug-drug interactions occur, resulting in the emergence of the emission peak at 369 nm.

FRET experiments were carried out to further confirm the mechanism of micellar solubilization using ATZ-curcumin as a FRET pair. Control experiments carried out on curcumin alone dissolved in 3.6 mg/mL SDS solution showed a very weak emission peak at 524 nm when excited at 250 and 328 nm, whereas an intense emission peak was observed when an excitation wavelength of 369 nm was used. Previous reports, based on the UV absorption spectrum of curcumin in media with varying polarity, suggest that curcumin alone in SDS is solubilized at the micelle corona/water interface (68). Similar experiments were carried out in this study wherein absorption spectra were obtained for curcumin alone in SDS solution, curcumin in the presence of 45 and 1200 μg/mL ATZ predissolved in SDS solution and curcumin in dodecane (data not shown). The absorption spectra of curcumin alone and curcumin in the presence of a low ATZ concentration suggested curcumin is dissolved at micelle/water interface, similar to reported literature (68). However, at high ATZ concentration, curcumin showed a hypsochromic shift with some spectral resemblance to curcumin in dodecane suggesting that in the presence of high ATZ concentration, curcumin partitions into the micellar core and is solubilized in less polar environment. Hence, it was hypothesized that at ATZ concentrations corresponding to Region I, where the fluorescence emission peak at 369 nm is not evident, no spectral emission from curcumin should be observed. However, at ATZ concentrations corresponding to Region II, which show an emission peak at 369 nm, energy transfer can occur from ATZ to curcumin if the separation distance between the molecules is small, resulting in an emission peak of curcumin. Figure 11 shows the FRET results. It is evident that at ATZ concentration of 45 μg/mL, no FRET process occurs from the drug to curcumin. When the ATZ concentration is increased to 1200 μg/mL, a FRET process occurs resulting in a curcumin emission peak at 500 nm. The hypsochromic shift for the curcumin UV absorption as well as fluorescence emission spectrum observed in the presence of ATZ coupled with the FRET process suggests co-localization of ATZ and curcumin in a non-polar environment. FRET experiments carried out for other ATZ concentrations consistently showed an absence of the curcumin emission peak for ATZ concentrations corresponding to Region I whereas, the curcumin peak was evident for drug concentrations corresponding to Region II. These observations further confirm the proposed mechanism of solubilization.

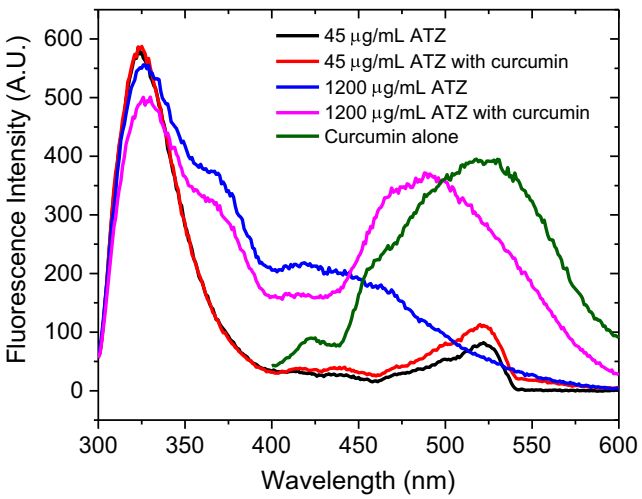

Fig. 11 FRET study of ATZ with curcumin in 3.6 mg/mL SDS solution. No FRET process occurs at low ATZ concentration whereas, FRET occurs at high ATZ concentration resulting in a curcumin emission peak.

Estimation of Number of ATZ Molecules per Micelle

N_{agg} which gives the number of surfactant monomer molecules present in a micelle was used to determine total number of micelles formed at different surfactant concentrations. To determine the number of ATZ molecules per micelle, the amount of drug present in the micelle was estimated as described above, and then divided by the total number of micelles in the solution. Figure 12 shows the number of drug molecules/micelle as a function of $SR_{activity}$ for the three different surfactant concentrations. From Fig. 12, it can be seen that for a particular value of $SR_{activity}$, each micelle contains approximately the same number of drug molecules and the number of drug molecules per micelle increases with an increase in $SR_{activity}$ for each surfactant concentration. As the N_{agg} for SDS micelles remains approximately constant with SDS concentration, the extent to which drug molecules are solubilized at a particular SR by each micelle remains constant, while the

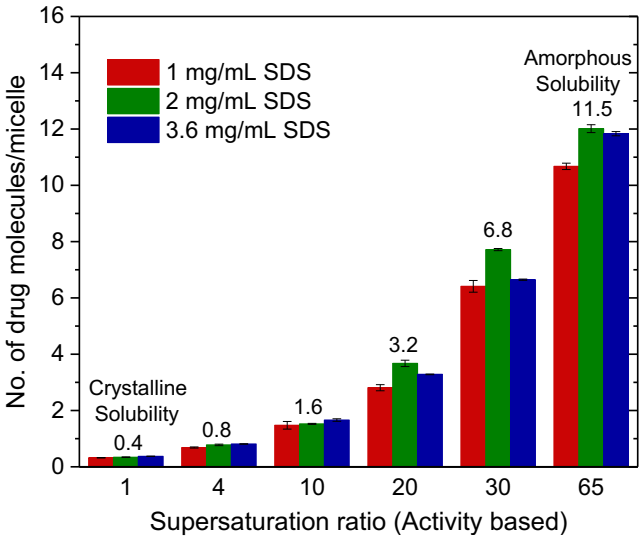

Fig. 12 Estimation of number of ATZ molecules in each micelle at different levels of supersaturation in the presence of varying SDS concentrations. Each micelle contains approximately the same number of molecules at a given supersaturation ratio for different SDS concentrations. The numbers above the data points are the mean values obtained for the three SDS concentrations.

number of micelles increases with increasing SDS concentration, resulting in enhanced solubilization at higher SDS concentration. Thus when a significant number of ATZ molecules are solubilized in individual micelles, the size of the micelles is expected to increase appreciably, which will be discussed in the next section.

Size Determination of SDS Micelles

The size of the SDS micelles was estimated using D_{NMR} obtained from PGSE-NMR and employing the Stokes-Einstein equation. This study was carried out to determine the impact of ATZ concentration on the size of the micelle, and hence provide insight into the solubilization mechanism. Here, 40 mg/mL SDS was used and experiments were carried out at 25°C. High SDS concentration was employed to minimize the contribution of SDS monomers to the diffusion measurements of SDS micelles which may negatively skew the results. First, diffusion of SDS micelles was determined in the absence of the drug to determine the size of the micelles. Next, two ATZ concentrations were studied- 1) 0.4 mg/mL whereby the drug is expected to be solubilized by adsorption and 2) 7 mg/mL which is expected to lead to solubilization in the micelle core. Table III summarizes the D_{NMR} values and the size of the micelles in the presence and absence of drug. It can be seen that at a drug concentration of 0.4 mg/mL the size of drug-containing micelle is equal to that of an empty micelle whereas, at a drug concentration of 7 mg/mL, the size of the micelle by volume increases by 130% compared to an empty micelle. The increase in observed volume agrees well with the theoretical 100% increase which was estimated based on the size of an atazanavir molecule in a close-packed crystal. This can be explained based on the number of drug molecules/micelle and the mechanism of solubilization. At the lower drug concentration, each micelle solubilizes ~0.4 drug molecules by adsorption at the micelle/water interface and thus, the drug molecules do not lead to an increase in micelle size, whereas at a concentration of 7 mg/mL, each micelle solubilizes ~7 drug molecules by solubilization in the core resulting in expansion of the micelle to accommodate the drug. Further, the D_{NMR} values of ATZ in the presence of SDS were equal to those of SDS, confirming that the drug is associated with the micelle.

Table III Self Diffusion Coefficient and Size of the SDS Micelles in Presence of Different ATZ Concentrations

Drug concentration (mg/ml)	0	0.4	7
D_{NMR} (m^2/s)	$10^{-10.3}$	$10^{-10.3}$	$10^{-10.42}$
r (nm)	4.61	4.61	6.08

DISCUSSION

Supersaturation and Amorphous Solubility in Presence of Surfactants

Surfactants present in the formulation, dissolution medium or in the intestinal fluids can enhance the solubility of drugs. The extent and mechanism of solubilization of the surfactant towards a solute can vary for different surfactant-solute combinations (69,70). A measure of the extent of solubilization is the solubilizing power (κ). κ is typically determined by measuring the increase in solubility of the crystalline form of the drug, applying Eq. 6. A related parameter is the micelle/water partition coefficient ($K_{m/w}$) which is also typically determined at saturation. However, very little is known about solubilization mechanisms in supersaturated solutions. The extent of supersaturation is typically calculated from the ratio of the concentration in the solution of interest to the concentration of a saturated solution in the same medium; this approach assumes that the concentration ratio provides a good surrogate for the activity ratio as shown in Eq. 9. For this approximation to hold true in supersaturated solutions containing micelles, the micelle/water partition coefficient needs to be constant over the concentration range of interest. Based on the data shown in Fig. 8, it is clear that the $K_{m/w}$ for the atazanavir:SDS is highly dependent on the concentration of the solute. Hence, we might expect that a *SR* based on the concentration ratio will yield a different number from a measure of supersaturation that depends on the solute activity. Conveniently, flux measurements can be used to evaluate changes in solute activity and hence supersaturation as a function of solution concentration and composition (35,45). For example, it has been demonstrated that for the same total solute concentration, the solute activity is lowered (reduced flux across a membrane) in a supersaturated solution containing surfactant micelles relative to that in the micelle-free solution (45). In agreement with previous observations, we find that using concentration ratios to evaluate supersaturation in the presence of micelles yields erroneous estimates of the supersaturation, and in the case of the ATZ:SDS system, grossly under-predicts the true supersaturation of the system as clearly demonstrated in Fig. 7. If the crystalline state is considered to have an activity of 1, based on the calculations described above (Eq. 3), the activity of water-saturated amorphous ATZ is estimated to be 65. Therefore, the flux of a solution at the amorphous solubility is expected to be approximately 65 times higher than that of a solution at the crystalline solubility, regardless of the total solution concentration. This assumption should hold true as long as the activity of the amorphous drug is not reduced by mixing with other dissolved components. By referring to the data shown in Fig. 7 in the presence of micellar SDS it is apparent that: 1) the free drug concentration varies between 1 μg/mL at the crystalline solubility and 65 μg/mL at the amorphous solubility and activity

ranges from 1 to 65 in both buffer and solutions containing different surfactant concentration as anticipated, whereas, the total drug concentration increases with increasing surfactant concentration. This observation confirms that, 1) while SDS micelles solubilize the drug accounting for the increase in concentration, SDS does not mix with the drug-rich phase which is formed when the initial activity of the solute in the solution exceeds a value of 65; if SDS mixed with the drug-rich phase, the activity and hence the maximum flux observed would be lowered (71); 2) the maximum $SR_{activity}$ observed is ~65, regardless of the SDS concentration, and is very similar to the predicted amorphous-to-crystal solubility ratio; 3) at the amorphous solubility, SR_{conc} underestimates the supersaturation by a factor of nearly two. At concentrations intermediate to the crystalline and amorphous solubility, SR_{conc} also underestimates the supersaturation. These results demonstrate that concentration ratios cannot be used to provide an accurate estimate of supersaturation in the ATZ:SDS system, even when the solubilization of the crystalline form is taken into account. Given that this is a common practice amongst pharmaceutical scientists, this is clearly an important finding.

As the activity of the drug in solution in equilibrium with different phases of ATZ (i.e. crystalline or water-saturated amorphous ATZ) is not impacted by surfactant molecules, the $SR_{activity}$ at the amorphous solubility is a constant and equal to that obtained in neat buffer. This can be readily ascertained by confirming that the maximum flux obtainable from surfactant-containing solutions at the amorphous solubility is ~65 higher than those at the crystalline solubility. Confidence in these results is provided by the observation that the flux ratio is also equal to the predicted amorphous-to-crystal solubility ratio. Thus, Eq. 3 can be employed to predict the supersaturation ratio but cannot be used to predict amorphous-to-crystal solubility ratio in presence of surfactants. From Eqs. 2 and 3, it is apparent that the predicted solubility ratio depends on the thermodynamic properties such as melting temperature of the crystalline solid, its heat of fusion and the amount of moisture absorbed by the amorphous solid. The implicit assumption is that the thermodynamic activity of the reference phases (i.e. amorphous and crystalline ATZ) does not change with solution composition, an assumption that holds true in the current study. However, the use of concentrations in Eq. 3 is only valid if the activity coefficients are the same at the amorphous and crystalline solubilities. This approximation appears to hold true in simple media based on the good agreement observed between predicted and experimental amorphous solubility values (37,72). However, it clearly breaks down for atazanavir in the presence of SDS surfactant micelles. Hence the amorphous-crystalline solubility advantage appears to be reduced by a factor of two in the presence of SDS micelles, based on the concentration ratios of the amorphous and crystalline solubilities. However, the flux measurements clearly show that, at the amorphous solubility, the solution has the same activity and supersaturation regardless of the presence or absence of micelles.

To understand the origin of the discrepancy between $SR_{activity}$ and SR_{conc}, we note that the solubilizing power of SDS for ATZ at a concentration equivalent to the amorphous solubility is only approximately half of that expected based on the solubilizing power calculated for saturated solutions and the solubility ratio predicted using Eq. 3. This discrepancy between the predicted and the experimental amorphous solubility values (Fig. 4) can be attributed to a changing value of the micelle/water partition coefficient as a function of ATZ concentration, which in turn is related to a concentration dependent change in the solubilization mechanism. At lower concentrations that are close to the crystalline solubility, the drug is solubilized by adsorption at the micelle/water interface, whereas, when the solution is supersaturated, the drug is solubilized in the hydrophobic core. Such a change in solubilization mechanism has been previously observed for solubilization of benzene by cetyltrimethylammonium bromide micelles, wherein, at low benzene concentration, nuclear magnetic resonance (NMR) studies suggested that the compound is solubilized at the surface of the micelle while at the high concentrations, the compound is solubilized in the core of the micelle (48). Mukherjee and Cardinal proposed a "two-state" model to explain the observation with benzene. According to this model, at low concentrations, benzene exists in an "adsorbed state" at the micelle/water interface, while at high concentrations, it is believed to be in a "dissolved state" in the hydrophobic core (73). This dissolution-adsorption model for solubilization by micelles is also observed in this study. As the predicted amorphous solubility calculation is based on the crystalline solubility, this prediction inherently assumes that, in supersaturated solutions of ATZ, the drug is solubilized by the same mechanism in a saturated solution i.e. by the adsorption mechanism; this is clearly not true in the case of ATZ, and is likely to be a problematic assumption for other compounds. This means that neither the amorphous solubility nor the supersaturation ratio can be estimated in presence of surfactants by measuring the increase in crystalline solubility. A change in solubilization mechanism results in a change in $K_{m/w}$ as shown in Fig. 8. There are several literature reports that document that $K_{m/w}$ is not necessarily a constant value and can increase (74), decrease (65) or remain a constant (67) depending on the polarity of the solute and interactions between the solute and the surfactant. Herein, it was observed that $K_{m/w}$ varied depending on the total drug concentration and the location of solubilization. At low ATZ concentration, (region I, Fig. 8) $K_{m/w}$ decreases with total drug concentration and this can be explained based on an adsorption solubilization mechanism. As the drug is added to the micellar solution, it becomes adsorbed at the micelle/water interface. As more and more drug gets adsorbed on the micellar surface, fewer sites are available for further adsorption. This leads to a decrease in

the amount of drug on the micelle relative to that in the water, resulting in decrease in $K_{m/w}$ at higher drug concentrations. For a constant surfactant concentration, further increase in drug concentration up to the amorphous solubility leads to a plateau in $K_{m/w}$ (Region II). Such a plateau has been related in previous reports to solubilization of the drug by dissolution in the hydrophobic core of the micelle (67). In this study, the micellar core of the SDS micelles is composed of dodecyl chains. Here, a balance exist between the drug solubilized by the hydrophobic dodecyl chains and the unbound drug in the aqueous compartment leading to a constant $K_{m/w}$. The change in solubilization mechanism from adsorption at the surface to dissolution in the core is also supported by the fluorescence experiments. Furthermore, PGSE-NMR studies demonstrate that this change in mechanism of solubilization also leads to an increase in the micelle size, although not aggregation number. The changes in solubilization location at different drug concentrations along with the impact on micelle size is summarized in schematic form in Fig. 13.

The amorphous solubility marks the maximum solubility of a solute in a given medium; above the amorphous solubility, the system will tend to undergo liquid-liquid or glass-liquid phase separation. At this concentration, each SDS micelle can solubilize ~11 ATZ molecules while 70 μg/mL of the drug is present as molecularly dissolved drug in the aqueous compartment. Thus, each SDS micelle has a finite capacity to solubilize the drug molecules (11 molecules in this case) and when this limit is exceeded such that no more drug can be solubilized by the micelle, the system undergoes LLPS and the drug subsequently exists in three different states − molecularly dissolved drug in the aqueous compartment, drug solubilized in the micelle and drug in the water saturated drug-rich phase. Thus, given the complexity of drug solubilization as a function of concentration, it becomes a non-trivial endeavor to predict how supersaturation varies as a function of added drug concentration whereby factors such as solubilization mechanisms, $K_{m/w}$ and carrying capacity of the micelle must be taken into consideration.

From Fig. 12 which gives the number of drug molecules solubilized by each micelle, it is evident that for a given $SR_{activity}$, the number of drug molecules solubilized by each micelle for varying SDS concentrations remains constant since, in the case of SDS, the number of SDS monomers per micelle remains constant whereby the number of micelles increases with increasing surfactant concentration. Thus, if the number of drug molecules per micelle is known for a given surfactant concentration, it might be possible to extrapolate this to different surfactant concentrations. In other words, if the experimental amorphous solubility is known at one surfactant concentration, it may be possible to estimate the amorphous solubility for varying surfactant concentrations as long as the aggregation number does not change with concentration and there is no further change of solubilization mechanism.

As simultaneous solubilization and supersaturation is likely to occur with other low solubility compounds, it is worth discussing the generality of the results observed in this study. The ratio of 2:1 for predicted amorphous to experimental amorphous solubility and $SR_{activity}$ to SR_{conc} is most likely both compound and surfactant dependent. Coincidentally, Raina *et al.*, observed an approximately 2:1 $SR_{activity}$ to SR_{conc} ratio for the amorphous solubility of felodipine in the presence of micellar surfactants (45). However, Lu *et al.*, observed smaller deviations between $SR_{activity}$ to SR_{conc} for teleprevir in presence of micellar bile salts (75). Nonetheless, a common observation for all these systems, is that the presence of solubilizing additives leads to differences between the concentration and activity based supersaturation values. It is expected that in cases where surfactant concentration is lower than the CMC or the

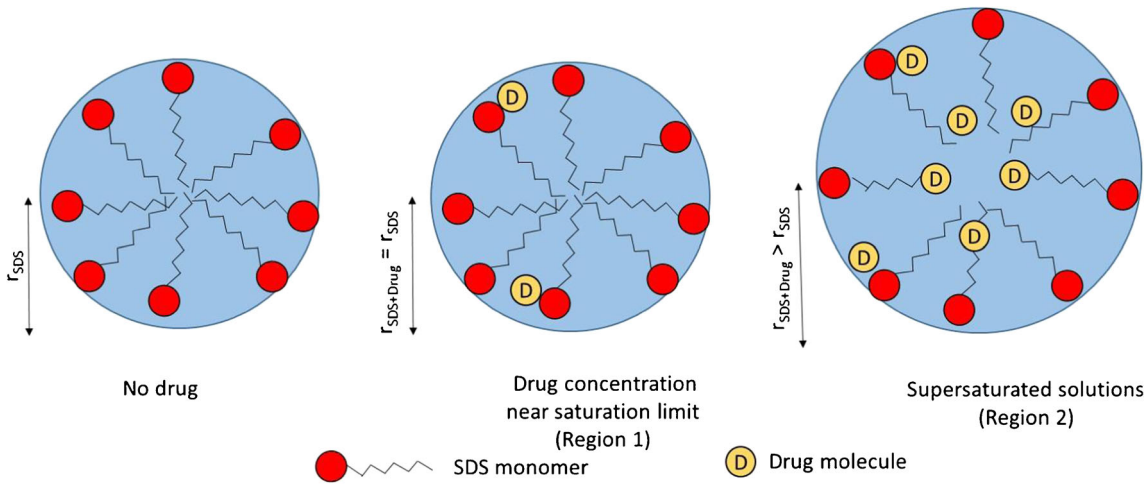

Fig. 13 Schematic representing mechanism and location of solubilization of ATZ in SDS micelle with change in size at different degrees of supersaturation .Note: Drug not drawn in proportion to SDS monomer.

solubilizing capacity of the surfactant is negligible, the ratio of $SR_{activity}$ to SR_{conc} will be closer to 1. In such cases simple concentration based SRs can be safely employed. In contrast, compounds effectively solubilized by surfactant micelles are expected to result in larger deviations between $SR_{activity}$ and SR_{conc}.

Implications of Erroneous Measurements of S on Evaluating Product Performance

Supersaturated systems can be formed *in vivo* via dissolution of enabling formulations such as an ASD (76,77) or a salt form (78), upon lipid digestion of the formulation excipients while employing self-emulsifying drug delivery systems (SEDDS) (10) or precipitation of weakly basic drugs in the intestinal fluids upon gastrointestinal transit (79). It is known that supersaturated solutions can provide enhanced membrane transport by increasing the number of molecules available for diffusion across membrane in comparison to formulations that that do not create supersaturation. As a result, such formulation strategies are gaining increasing interest especially in cases where absorption is limited by the poor solubility of the compound. However, as these solutions are metastable, they are also prone to undergo desupersaturation or crystallization thereby reducing solution concentration. Thus, for a formulation to exhibit the desired performance, it is critical that the solution remains supersaturated. The rate of permeation as well as the rate of desupersaturation depend on the extent of supersaturation. Hence, in order to appropriately compare and evaluate the performance of different formulations it is crucial to accurately determine the supersaturation.

As surfactants are incorporated in the ASDs to enhance their dissolution performance, it is of interest to understand the impact of erroneous measurements of supersaturation on formulation design and its performance. Consider formulation 1 that contains the amount of surfactant such that, upon complete dissolution of the ASD, the surfactant in the solution exceeds its CMC leading to solubilization of the drug. In this case, the free drug concentration will be less than the total solution concentration. In contrast, consider formulation 2 that does not contain a surfactant and undergoes complete dissolution at a relatively slower rate. Here, although the dissolution rate is slower, the solubility of the drug will not be impacted and the total solution concentration will be equal to the free drug concentration. A formulation scientist without an accurate knowledge of supersaturation may choose formulation 1 over 2 based on dissolution rate and total solution concentration. However, as the rate of membrane transport depends on supersaturation, which in turn is a function of free drug concentration alone, formulation 1 may exhibit slower rate of permeation *in vivo* compared to formulation 2. Thus, *in vitro* dissolution methods without accurate knowledge of supersaturation used to rank order formulations containing surfactants may lead to erroneous *in vivo* predictions.

In vitro permeability determination involves measuring flux across artificial membranes prepared by impregnating porous filter membranes with lipidic components such as hexadecane (80) or phospholipids (81), rendering them lipophilic, or by employing different cell-lines such as Caco-2 cells and determining the flux across a monolayer of cells (82,83). Apparent permeability (P_{app}) is then estimated by employing Eq. 12 (84). Here, C_0 is the initial donor concentration. $\frac{dm}{dtA}$ is the diffusive flux across the membrane as given in Eq. 4.

$$P_{app} = \frac{dm}{dtAC_0} \tag{12}$$

An important caveat here is that the equation uses concentration differences between donor and acceptor compartments instead of activity differences. Eq. 12 can give satisfactory results when $\gamma = 1$ or $\gamma/\gamma^* = 1$. To demonstrate the magnitude of errors in permeability measurements when employing Eq. 12 in the presence of solubility enhancing additives, permeability was determined from the flux data obtained in this study using both activity and concentration in presence of 3.6 mg/mL SDS. It was observed that when activity was employed, the permeability was same as that obtained in buffer. However, permeability was 20 fold lower when total concentration in the donor cell was employed, which is implausible as permeability is a property of the molecule and should remain constant for a particular membrane, temperature and hydrodynamic conditions as long as the additives do not modify the membrane properties. This discrepancy was observed in the work by Miller *et al.* The authors concluded that the solubilizing additives reduced apparent permeability as it was determined based on total solubility in the presence of surfactants rather than the free drug concentration (17–20). A mechanistic model was developed by Miller *et al.* to predict impact of micellar solubilization on intestinal permeation (17). Here, the surfactant-related factors that can impact the permeability are surfactant concentration and the association constant between the micelle and the drug. This association constant may vary with the permeant (drug) concentration and as a result, the permeability predicted at one concentration may not be extended to other concentrations. Previous reports on the impact of solubilizing additives on the intestinal permeability have also attributed the decrease in permeability due to solubility enhancement to a reduction in the free fraction of drug (85). Katneni *et al.* suggested a reciprocal permeability approach to determine permeability in presence of solubilizing additives which takes into consideration the free fraction of drug available for transport (86). However, this approach assumes a constant $K_{m/w}$, which in this study was found to vary based on mechanism of solubilization. Thus, such predictions may or may not simulate the experimental results accurately and hence, must be used with caution.

Formulation Design, Surfactants and LLPS

Surfactants are often added to an ASD to improve wetting and dissolution of the formulation. These surfactants can enhance solubility and thus impact supersaturation. As observed in this study, enhancement in solubility can result in a decrease in free drug leading to a reduction in supersaturation. As diffusive flux directly depends on the amount of free drug available for permeation, solubilization can result in a decrease in flux in comparison to a formulation that does not exhibit a solubilization effect, under the assumption that the total concentration in both cases is equal. Further, it has been shown that certain formulations, depending on the polymer type and drug-to-polymer ratio, can undergo LLPS upon dissolution when the amorphous solubility is exceeded (76,77). The amorphous nanodroplets formed upon LLPS may be advantageous for passive diffusion *in vivo* as these nanodroplets have been shown to serve as a reservoir of drug thus replenishing any absorbed drug from the continuous phase to keep the solution concentration and drug activity at their maxima leading to sustainment of flux at a maximum value. This reservoir effect is not observed when the precipitated phase is in the form of micron sized amorphous solid particles (36). Therefore, for compounds that are absorbed by passive diffusion, maximum performance can be achieved if the formulation undergoes LLPS. It can be argued that drug solubilized in the micelle can also serve as a reservoir to replenish the free drug that is absorbed from the aqueous compartment depending on the $K_{m/w}$. While this is true, it must be remembered that the diffusive flux depends on the free drug concentration. A system that has undergone LLPS will exhibit sustained maximum flux, whereas a system with the same total concentration but in which drug is solubilized by the micelles such that the activity is lower, will exhibit lower flux. These differences may play a more significant role for the compounds with a narrow absorption window. Thus, a formulation must be designed such that it takes into account the amorphous solubility of the drug and potential to undergo LLPS. Further, the amount of additives in the formulation can be chosen such that they improve dissolution and wetting but do not form structures that can solubilize the drug. In addition to the surfactants in the formulation, bile salts and phospholipids in the intestinal fluids form micelles, mixed micelles and vesicles which can also enhance solubility. As a result, the amorphous solubility of the drug must be determined in these relevant media and the formulation should be designed to undergo LLPS if possible, taking into consideration the impact of the additives as well as components of the intestinal fluids.

CONCLUSIONS

The observed amorphous-to-crystalline solubility ratio of atazanavir in the presence of sodium dodecyl sulfate micelles was found to be approximately half of that in surfactant-free buffer. At first glance, this observation suggests that SDS micelles reduce the amorphous solubility advantage, however diffusive flux measurements showed that this was an erroneous conclusion. Flux measurements clearly showed that the supersaturation in the presence of SDS micelles did not scale with the concentration ratio, leading to the important conclusion that, for this system, concentration measurements cannot be used to evaluate the degree of supersaturation. The mechanistic basis for these observations is a change in solubilization mechanism as a function of solute concentration which leads to a corresponding dependence of the micelle/water partition coefficient on solute concentration. As solute thermodynamic activity, rather than concentration, drives important processes such as crystallization and permeation across a membrane, an improved understanding of solution thermodynamics is an essential tool in developing enabling formulations. In particular, rigorous methodology needs to be employed when evaluating supersaturation in complex media where solubilizing additives are present.

ACKNOWLEDGMENTS AND DISCLOSURES

We would like to acknowledge AbbVie Inc. for providing research funding for this project. Purdue University and AbbVie jointly participated in study design, research, data collection, analysis and interpretation of data, writing, reviewing, and approving the publication. Anura S. Indulkar is a graduate student at Purdue University; Lynne S. Taylor is a professor at Purdue University; Huaping Mo is an Associate Director of Purdue Interdepartmental NMR Facility at Purdue University. They all have no additional conflicts of interest to report. Shweta A. Raina, Yi Gao, and Geoff G. Z. Zhang are employees of AbbVie and may own AbbVie stock.

REFERENCES

1. Hogan JC. Combinatorial chemistry in drug discovery. Nat Biotechnol. 1997;15(4):328–30.
2. Broach JR, Thorner J. High-throughput screening for drug discovery. Nature. 1996;384(6604 Suppl):14–6.
3. Carnero A. High throughput screening in drug discovery. Clin Transl Oncol. 2006;8(7):482–90.
4. Lipinski CA. Drug-like properties and the causes of poor solubility and poor permeability. J Pharmacol Toxicol Methods. 2000;44(1):235–49.
5. Lipinski CA, Lombardo F, Dominy BW, Feeney PJ. Experimental and computational approaches to estimate solubility and

permeability in drug discovery and development settings. Adv Drug Deliv Rev. 1997;23(1–3):3–25.
6. Ran Y, Zhao L, Xu Q, Yalkowsky SH. Solubilization of cyclosporin a. AAPS PharmSciTech. 2001;2(1):23–6.
7. Loftsson T, Magnúsdóttir A, Másson M, Sigurjónsdóttir JF. Self-association and cyclodextrin solubilization of drugs. J Pharm Sci. 2002;91(11):2307–16.
8. Müller BW, Brauns U. Solubilization of drugs by modified β-cyclodextrins. Int J Pharm. 1985;26(1):77–88.
9. Neslihan Gursoy R, Benita S. Self-emulsifying drug delivery systems (SEDDS) for improved oral delivery of lipophilic drugs. Biomed Pharmacother. 2004;58(3):173–82.
10. Anby MU, Williams HD, McIntosh M, Benameur H, Edwards GA, Pouton CW, Porter CJH. Lipid digestion as a trigger for supersaturation: evaluation of the impact of supersaturation stabilization on the in vitro and in vivo performance of self-emulsifying drug delivery systems. Mol Pharm. 2012;9(7):2063–79.
11. Williams HD, Trevaskis NL, Yeap YY, Anby MU, Pouton CW, Porter CJ. Lipid-based formulations and drug supersaturation: harnessing the unique benefits of the lipid digestion/absorption pathway. Pharm Res. 2013;30(12):2976–92.
12. Serajuddin ATM. Salt formation to improve drug solubility. Adv Drug Deliv Rev. 2007;59(7):603–16.
13. Thakuria R, Delori A, Jones W, Lipert MP, Roy L, Rodríguez-Hornedo N. Pharmaceutical cocrystals and poorly soluble drugs. Int J Pharm. 2013;453(1):101–25.
14. Newman A, Knipp G, Zografi G. Assessing the performance of amorphous solid dispersions. J Pharm Sci. 2012;101(4):1355–77.
15. Brouwers J, Tack J, Augustijns P. *In vitro* behavior of a phosphate ester prodrug of amprenavir in human intestinal fluids and in the Caco-2 system: illustration of intraluminal supersaturation. Int J Pharm. 2007;336(2):302–9.
16. Kapoor M, Siegel RA. Prodrug/enzyme based acceleration of absorption of hydrophobic drugs: an in vitro study. Mol Pharm. 2013;10(9):3519–24.
17. Miller JM, Beig A, Krieg BJ, Carr RA, Borchardt TB, Amidon GE, Amidon GL, Dahan A. The solubility–permeability interplay: mechanistic modeling and predictive application of the impact of micellar Solubilization on intestinal permeation. Mol Pharm. 2011;8(5):1848–56.
18. Miller JM, Beig A, Carr RA, Spence JK, Dahan A. A win–win solution in oral delivery of lipophilic drugs: supersaturation via amorphous solid dispersions increases apparent solubility without sacrifice of intestinal membrane permeability. Mol Pharm. 2012;9(7):2009–16.
19. Dahan A, Miller JM, Hoffman A, Amidon GE, Amidon GL. The solubility–permeability interplay in using cyclodextrins as pharmaceutical solubilizers: mechanistic modeling and application to progesterone. J Pharm Sci. 2010;99(6):2739–49.
20. Miller JM, Beig A, Carr RA, Webster GK, Dahan A. The solubility–permeability interplay when using Cosolvents for Solubilization: revising the way we use solubility-enabling formulations. Mol Pharm. 2012;9(3):581–90.
21. Hou H, Siegel RA. Enhanced permeation of diazepam through artificial membranes from supersaturated solutions. J Pharm Sci. 2006;95(4):896–905.
22. Leveque N, Raghavan SL, Lane ME, Hadgraft J. Use of a molecular form technique for the penetration of supersaturated solutions of salicylic acid across silicone membranes and human skin *in vitro*. Int J Pharm. 2006;318(1–2):49–54.
23. Megrab NA, Williams AC, Barry BW. Oestradiol permeation through human skin and silastic membrane: effects of propylene glycol and supersaturation. J Control Release. 1995;36(3):277–94.
24. Pellett MA, Castellano S, Hadgraft J, Davis AF. The penetration of supersaturated solutions of piroxicam across silicone membranes and human skin *in vitro*. J Control Release. 1997;46(3):205–14.
25. Mullin JW. Solutions and solubility. In: Crystallization. Oxford: Butterworth-Heinemann; 2001. p. 86–134.
26. Higuchi T. Physical chemical analysis of percutaneous absorption process from creams and ointments. J Soc Cosmet Chem. 1960;11(2):85–97.
27. Twist J, Zatz J. Characterization of solvent-enhanced permeation through a skin model membrane. J Soc Cosmet Chem. 1988;39(5):324–4.
28. Sigurðoardóttir AM, Loftsson T. The effect of polyvinylpyrrolidone on cyclodextrin complexation of hydrocortisone and its diffusion through hairless mouse skin. Int J Pharm. 1995;126(1–2):73–8.
29. Loftsson T, Sigurðardóttir AM. The effect of polyvinylpyrrolidone and hydroxypropyl methylcellulose on HPβCD complexation of hydrocortisone and its permeability through hairless mouse skin. Eur J Pharm Sci. 1994;2(4):297–301.
30. Kim J-H, Choi H-K. Effect of additives on the crystallization and the permeation of ketoprofen from adhesive matrix. Int J Pharm. 2002;236(1–2):81–5.
31. Ilevbare GA, Taylor LS. Liquid–liquid phase separation in highly supersaturated aqueous solutions of poorly water-soluble drugs: implications for solubility enhancing formulations. Cryst Growth Des. 2013;13(4):1497–509.
32. Mosquera-Giraldo LI, Taylor LS. Glass–liquid phase separation in highly supersaturated aqueous solutions of Telaprevir. Mol Pharm. 2015;12(2):496–503.
33. Indulkar AS, Box KJ, Taylor R, Ruiz R, Taylor LS. pH-dependent liquid–liquid phase separation of highly supersaturated solutions of weakly basic drugs. Mol Pharm. 2015;12(7):2365–77.
34. Jackson MJ, Kestur US, Hussain MA, Taylor LS. Characterization of supersaturated Danazol solutions–impact of polymers on solution properties and phase transitions. Pharm Res. 2016;33(5):1–13.
35. Raina SA, Zhang GGZ, Alonzo DE, Wu J, Zhu D, Catron ND, Gao Y, Taylor LS. Enhancements and limits in drug membrane transport using supersaturated solutions of poorly water soluble drugs. J Pharm Sci. 103(9):2736–48.
36. Indulkar AS, Gao Y, Raina SA, Zhang GGZ, Taylor LS. Exploiting the phenomenon of liquid–liquid phase separation for enhanced and sustained membrane transport of a poorly water-soluble drug. Mol Pharm. 2016;13(6):2059–69.
37. Taylor LS, Zhang GGZ. Physical chemistry of supersaturated solutions and implications for oral absorption. Adv Drug Deliv Rev. 2016;101:122–42.
38. Jantratid E, Dressman J. Biorelevant dissolution media simulating the proximal human gastrointestinal tract: an update. Dissolution Technologies. 2009;16(3):21–5.
39. Dressman JB, Amidon GL, Reppas C, Shah VP. Dissolution testing as a prognostic tool for oral drug absorption: immediate release dosage forms. Pharm Res. 1998;15(1):11–22.
40. Riethorst D, Mols R, Duchateau G, Tack J, Brouwers J, Augustijns P. Characterization of human duodenal fluids in fasted and fed state conditions. J Pharm Sci. 2016;105(2):673–81.
41. Mazer NA, Benedek GB, Carey MC. Quasielastic light-scattering studies of aqueous biliary lipid systems. Mixed micelle formation in bile salt-lecithin solutions. Biochemistry. 1980;19(4):601–15.
42. Small DM, Penkett SA, Chapman D. Studies on simple and mixed bile salt micelles by nuclear magnetic resonance spectroscopy. Biochimica et Biophysica Acta, Lipids and Lipid Metabolism. 1969;176(1):178–89.
43. Hammad MA, Müller BW. Increasing drug solubility by means of bile salt–phosphatidylcholine-based mixed micelles. Eur J Pharm Biopharm. 1998;46(3):361–7.

44. Rosoff M, Serajuddin ATM. Solubilization of diazepam in bile salts and in sodium cholate-lecithin-water phases. Int J Pharm. 1980;6(2):137–46.
45. Raina SA, Zhang GG, Alonzo DE, Wu J, Zhu D, Catron ND, Gao Y, Taylor LS. Impact of solubilizing additives on supersaturation and membrane transport of drugs. Pharm Res. 2015;32(10):3350–64.
46. Feng S. Studies on drug solubilization mechanism in simple micelle systems. Dissertation, Lexington: University of Kentucky; 2009.
47. Rosen MJ, Kunjappu JT. Solubilization by solutions of surfactants: micellar catalysis. In: Surfactants and interfacial phenomena. Hoboken: Wiley; 2012. p. 202–34.
48. Eriksson J, Gillberg G. NMR-studies of the solubilization of aromatic compounds in cetyltrimethylammonium bromide solution II. Acta Chem Scand. 1966;20(8):2019–27.
49. Jobe DJ, Reinsborough VC, Wetmore SD. Sodium dodecyl sulfate micellar aggregation numbers in the presence of cyclodextrins. Langmuir. 1995;11(7):2476–9.
50. Hansson P, Jönsson B, Ström C, Söderman O. Determination of micellar aggregation numbers in dilute surfactant systems with the fluorescence quenching method. J Phys Chem B. 2000;104(15):3496–506.
51. Alargova R, Kochijashky I, Sierra M, Zana R. Micelle aggregation numbers of surfactants in aqueous solutions: a comparison between the results from steady-state and time-resolved fluorescence quenching. Langmuir. 1998;14(19):5412–8.
52. Malliaris A. Static fluorescence quenching in the study of micellar systems. In: Hoffmann H, editor. New trends in Colloid Science. New York City: Springer; 1987. p. 161–6.
53. Infelta PP. Fluorescence quenching in micellar solutions and its application to the determination of aggregation numbers. Chem Phys Lett. 1979;61(1):88–91.
54. Turro NJ, Yekta A. Luminescent probes for detergent solutions. A simple procedure for determination of the mean aggregation number of micelles. J Am Chem Soc. 1978;100(18):5951–2.
55. Hoffman JD. Thermodynamic driving force in nucleation and Growth processes. J Chem Phys. 1958;29(5):1192–3.
56. Murdande SB, Pikal MJ, Shanker RM, Bogner RH. Solubility advantage of amorphous pharmaceuticals: I. A thermodynamic analysis. J Pharm Sci. 2010;99(3):1254–64.
57. Murdande SB, Pikal MJ, Shanker RM, Bogner RH. Solubility advantage of amorphous pharmaceuticals: II. Application of quantitative thermodynamic relationships for prediction of solubility enhancement in structurally diverse insoluble pharmaceuticals. Pharm Res. 2010;27(12):2704–14.
58. Purohit HS, Taylor LS. Phase separation kinetics in amorphous solid dispersions upon exposure to water. Mol Pharm. 2015;12(5):1623–35.
59. Fuguet E, Ràfols C, Rosés M, Bosch E. Critical micelle concentration of surfactants in aqueous buffered and unbuffered systems. Anal Chim Acta. 2005;548(1–2):95–100.
60. Corrin ML. The effect of salts and chain length on the critical concentrations of colloidal electrolytes. J Colloid Sci. 1948;3(4):333–8.
61. Tamori K, Watanabe Y, Esumi K. The partitioning of pyrene-3-carboxaldehyde at the micelle/bulk interface estimated by the fluorescence method. Langmuir. 1992;8(9):2344–6.
62. Phillips J. The energetics of micelle formation. Trans Faraday Soc. 1955;51:561–9.
63. Quina FH, Nassar PM, Bonilha JBS, Bales BL. Growth of sodium dodecyl sulfate micelles with detergent concentration. J Phys Chem. 1995;99(46):17028–31.
64. Florence AT, Attwood D. Surfactants. In: Physicochemical principles of pharmacy. London: Macmillan Education UK; 1998. p. 199–251.
65. Lee BH, Christian SD, Tucker EE, Scamehorn JF. Solubilization of mono-and dichlorophenols by hexadecylpyridinium chloride micelles. Effects of substituent groups. Langmuir. 1990;6(1):230–5.
66. Choucair A, Eisenberg A. Interfacial Solubilization of model amphiphilic molecules in block copolymer micelles. J Am Chem Soc. 2003;125(39):11993–2000.
67. Croy SR, Kwon GS. Polysorbate 80 and Cremophor EL micelles deaggregate and solubilize nystatin at the core–corona interface. J Pharm Sci. 2005;94(11):2345–54.
68. Adhikary R, Carlson PJ, Kee TW, Petrich JW. Excited-state intramolecular hydrogen atom transfer of curcumin in surfactant micelles. J Phys Chem B. 2010;114(8):2997–3004.
69. Moroi Y, Mitsunobu K, Morisue T, Kadobayashi Y, Sakai M. Solubilization of benzene, naphthalene, anthracene, and pyrene in 1-Dodecanesulfonic acid micelle. J Phys Chem. 1995;99(8):2372–6.
70. Gadelle F, Koros WJ, Schechter RS. Solubilization isotherms of aromatic solutes in surfactant aggregates. J Colloid Interface Sci. 1995;170(1):57–64.
71. Powell JJ, Faria N, Thomas-McKay E, Pele LC. Origin and fate of dietary nanoparticles and microparticles in the gastrointestinal tract. J Autoimmun. 2010;34(3):J226–33.
72. Jani P, Halbert GW, Langridge J, Florence AT. Nanoparticle uptake by the rat gastrointestinal mucosa: quantitation and particle size dependency. J Pharm Pharmacol. 1990;42(12):821–6.
73. Mukerjee P, Cardinal JR. Benzene derivatives and naphthalene solubilized in micelles. Polarity of microenvironments, location and distribution in micelles, and correlation with surface activity in hydrocarbon-water systems. J Phys Chem. 1978;82(14):1620–7.
74. Smith GA, Christian SD, Tucker EE, Scamehorn JF. Solubilization of hydrocarbons by surfactant micelles and mixed micelles. J Colloid Interface Sci. 1989;130(1):254–65.
75. Lu J, Ormes JD, Lowinger M, Xu W, Mitra A, Mann AK, Litster JD, Taylor LS. Impact of endogenous bile salts on the thermodynamics of supersaturated active pharmaceutical ingredient solutions. Cryst Growth Des. 2017;17(3):1264–75.
76. Alonzo DE, Gao Y, Zhou D, Mo H, Zhang GGZ, Taylor LS. Dissolution and precipitation behavior of amorphous solid dispersions. J Pharm Sci. 2011;100(8):3316–31.
77. Jackson MJ, Kestur US, Hussain MA, Taylor LS. Dissolution of Danazol amorphous solid dispersions: supersaturation and phase behavior as a function of drug loading and polymer type. Mol Pharm. 2016;13(1):223–31.
78. Almeida e Sousa L, Reutzel-Edens SM, Stephenson GA, Taylor LS. Supersaturation potential of salt, co-crystal, and amorphous forms of a model Weak Base. Cryst Growth Des. 2016;16(2):737–48.
79. Carlert S, Pålsson A, Hanisch G, Von Corswant C, Nilsson C, Lindfors L, Lennernäs H, Abrahamsson B. Predicting intestinal precipitation—a case example for a basic BCS class II drug. Pharm Res. 2010;27(10):2119–30.
80. Wohnsland F, Faller B. High-throughput permeability pH profile and high-throughput alkane/water log P with artificial membranes. J Med Chem. 2001;44(6):923–30.
81. Liu H, Sabus C, Carter GT, Du C, Avdeef A, Tischler M. *In vitro* permeability of poorly aqueous soluble compounds using different Solubilizers in the PAMPA assay with liquid chromatography/mass spectrometry detection. Pharm Res. 2003;20(11):1820–6.
82. Borchardt RT, Hidalgo I, Raub T, Borchardt R. Characterization of the human colon carcinoma cell line (Caco-2) as a model system for intestinal epithelial permeability. Gastroenterol. 1989;96(3):736–49.

83. Artursson P, Karlsson J. Correlation between oral drug absorption in humans and apparent drug permeability coefficients in human intestinal epithelial (Caco-2) cells. Biochem Biophys Res Commun. 1991;175(3):880–5.
84. Hubatsch I, Ragnarsson EGE, Artursson P. Determination of drug permeability and prediction of drug absorption in Caco-2 monolayers. Nat Protoc. 2007;2(9):2111–9.
85. Poelma FGJ, Breäs R, Tukker JJ, Crommelin DJA. Intestinal absorption of drugs. The influence of mixed micelles on on the disappearance kinetics of drugs from the small intestine of the rat. J Pharm Pharmacol. 1991;43(5):317–24.
86. Katneni K, Charman SA, Porter CJH. Permeability assessment of poorly water-soluble compounds under solubilizing conditions: the reciprocal permeability approach. J Pharm Sci. 2006;95(10):2170–85.